



OPEN ACCESS

EDITED BY

Dongri Song,
Chinese Academy of Sciences (CAS), China

REVIEWED BY

Mohammad Azarafza,
University of Tabriz, Iran
Kadir Gezici,
Atatürk Üniversitesi, Türkiye

*CORRESPONDENCE

Riheb Hadji,
✉ hadjirihab@gmail.com

RECEIVED 23 October 2025

REVISED 11 December 2025

ACCEPTED 12 December 2025

PUBLISHED 28 January 2026

CITATION

Gueffaf A, Hadji R, Faqeih K, Alamri SM, Alamery E, Aldubehi MA, Alamry JY and Fehdi C (2026) Geospatial assessment and mapping of water-induced soil erosion in a semiarid region of the MENA using GIS-based RUSLE modeling.


Front. Earth Sci. 13:1731125.

doi: 10.3389/feart.2025.1731125

COPYRIGHT

© 2026 Gueffaf, Hadji, Faqeih, Alamri, Alamery, Aldubehi, Alamry and Fehdi. This is an open-access article distributed under the terms of the [Creative Commons Attribution License \(CC BY\)](https://creativecommons.org/licenses/by/4.0/). The use, distribution or reproduction in other forums is permitted, provided the original author(s) and the copyright owner(s) are credited and that the original publication in this journal is cited, in accordance with accepted academic practice. No use, distribution or reproduction is permitted which does not comply with these terms.

Geospatial assessment and mapping of water-induced soil erosion in a semiarid region of the MENA using GIS-based RUSLE modeling

Ahmed Gueffaf^{1,2}, Riheb Hadji ^{3,4*}, Khadeijah Faqeih⁵, Somayah Moshrif Alamri⁵, Eman Alamery⁵, Maha Abdullah Aldubehi⁵, Jamilah Yahya Alamry⁵ and Chemsedine Fehdi^{1,2}

¹Department of Earth Sciences, Faculty of Exact Sciences, Natural and Life Sciences Echahid Cheikh Larbi Tebessi University, Tebessa, Algeria, ²Water and Environment Laboratory, Larbi Tebessi University, Tebessa, Algeria, ³Department of Earth Sciences, Institute of Architecture and Earth Sciences, Ferhat Abbas University, Setif, Algeria, ⁴Laboratory of Applied Research in Engineering Geology, Geotechnics, Water Sciences, and Environment, Ferhat Abbas University, Setif, Algeria, ⁵Department of Geography and Environmental Sustainability, College of Humanities and Social Sciences, Princess Nourah bint Abdulrahman University, Riyadh, Saudi Arabia

Soil erosion is a major environmental issue throughout the Middle East and North Africa, where it contributes to accelerated land degradation, declining soil fertility, and increased sediment accumulation in reservoirs. These pressures are especially pronounced in the Upper-Bousselam Watershed, an area of strategic importance for cereal production. The present study seeks to quantify the spatial patterns and annual rates of water-induced soil loss in this watershed in order to support more effective land-management and erosion-control strategies. Soil loss was estimated using a GIS-based implementation of the Revised Universal Soil Loss Equation. Spatial datasets describing rainfall erosivity, soil erodibility, topographic conditions, vegetation cover, and conservation practices were compiled and integrated to produce a basin-wide map of potential soil erosion. The analysis reveals a marked spatial heterogeneity in erosion intensity across the watershed. The highest soil-loss rates occur mainly in the northern mountainous areas and on certain southern slopes, where steep gradients, weak and easily erodible lithologies, and limited vegetation cover prevail. A general decrease in rainfall erosivity from north to south further accentuates these contrasts. Estimated annual soil losses range from very low values to more than 33 t/ha/year. Although nearly two-thirds of the basin is characterized by low erosion levels, about 9% of the area is subject to severe soil degradation. These results underline the combined role of climatic forcing, topography, lithology, and land cover in controlling erosion processes within the Upper-Bousselam Watershed. The spatially explicit erosion assessment provides a sound scientific basis for identifying priority areas for conservation measures

and supports efforts aimed at safeguarding soil resources and ensuring the long-term sustainability of agricultural production.

KEYWORDS

rainfall erosivity, RUSLE, soil erodibility, sustainable land conservation, topographic factor

1 Introduction

Soil erosion remains one of the most pressing global environmental challenges, with profound implications for agricultural productivity, food security, and ecosystem resilience (Rhodes, 2014; Sartori et al., 2024; Mi et al., 2025). Its effects are particularly pronounced in semi-arid regions, where the combined influence of climatic variability, unsustainable land management, and accelerated land-use change intensifies surface degradation (Khanchoul et al., 2020; Chakraborty et al., 2025). The gradual removal of fertile topsoil diminishes agricultural yields, promotes sediment accumulation in reservoirs, and deteriorates water quality and aquatic ecosystems (Lizaga et al., 2025).

In Algeria, water-induced erosion is recognized as one of the principal drivers of land degradation, especially in the northern regions characterized by steep slopes, dense population, and a significantly degraded vegetation cover (Mahleb et al., 2022; Hadji et al., 2025; Taib et al., 2024; 2025). Numerous studies have highlighted not only the magnitude of this phenomenon but also its irregular and spatially discontinuous nature (Benaiche et al., 2024). Approximately 45% of Algeria's arable land has already been affected by erosion processes. Nearly 50 million tons of suspended sediments are deposited annually along the country's Mediterranean coastline (Probst, 1992; Morsli et al., 2006; Nehaï, and Guettouche, 2020). A survey conducted by the Ministry of Agriculture and Rural Development reported that around 15 million hectares in northern Algeria have experienced severe soil degradation due to hydrological erosion.

Conventional approaches for assessing erosion (such as field surveys, runoff plot experiments, and empirical or physically based models) have generated valuable understandings into erosion mechanisms and rates (Bueno-Hurtado and Seidou, 2024). However, these methods are often constrained by their labor-intensive nature, high cost, and limited spatial representativeness (Ketema and Dwarakish, 2021).

The emergence of Geographic Information System (GIS) and remote sensing (RS) has revolutionized erosion research by enabling continuous, large-scale spatial analysis using geo-environmental indicators such as rainfall patterns, vegetation cover, land use, and topography (Abdo, 2022; Hamed et al., 2024).

Several researchers have significantly advanced the understanding of mass-wasting processes across varied geological and climatic contexts. Machine-learning approaches, including support vector machines (SVM), artificial neural networks (ANN), random forests (RF), and logistic regression, have been effectively applied to map susceptibility in hilly regions (Dahoua et al., 2017; Zerzour et al., 2020; Ahadi and Rosta, 2024; Abgrami et al., 2025), capturing complex spatial patterns of slope instability. Logistic regression and multi-criteria decision-making methods (AHP) have also been used to provide robust, site-specific assessments

in Maragheh and Fuman counties (Cemiloglu et al., 2023; Hamed et al., 2025). Complementing these modeling efforts, Yeganeh et al. (2025) developed a comprehensive landslide inventory for the Alborz Mountains, supporting hazard modeling and risk evaluation. Beyond landslides, advanced computational approaches have been successfully integrated with GIS to map rockfall susceptibility, as shown by Nanehkaran et al. (2022). Together, these studies provide technically rigorous, modern frameworks that enhance predictive accuracy and support effective hazard management across diverse environmental settings.

The availability of Digital Elevation Models (DEMs) and multi-temporal satellite imagery has further enhanced the capacity to identify erosion-prone areas, and monitor landscape evolution, (Huang et al., 2023). Despite these advances, several limitations persist. The spatial and vertical resolution of existing DEMs, and the lack of field-based validation data continue to reduce the reliability of erosion predictions, particularly in mountainous and data-scarce regions (Li et al., 2021). Moreover, while various models; including empirical approaches such as USLE, RUSLE, and MUSLE (Ghosal and Das Bhattacharya, 2020), as well as physically based ones like Unit Power-Based Soil Erosion and Deposition (USPED) have been widely applied across different environments (Prasad et al., 2024). Their performance often varies depending on local geomorphological, climatic, and land-use conditions (Wischmeier, 1959; Stocking and Elwell, 1973; Lo and MacKinlay, 1985). The RUSLE model is one of the most widely used tools for assessing soil erosion due to its flexibility and computational simplicity, making it suitable for studies with limited data and the absence of precise field measurements (Kouli et al., 2009). Numerous studies have shown that RUSLE's ability to integrate with Geographic Information Systems (GIS) and remote sensing techniques provides high efficiency in producing accurate spatial erosion maps over large areas (Panagos et al., 2015). Compared to models such as WEPP and EUROSEM, RUSLE requires fewer input data and remains applicable in mountainous and semi-arid environments where detailed information is difficult to obtain (Renard and Freimund, 1994). However, as an empirical model, its accuracy may be affected by environmental and climatic variations unless its factors are locally calibrated (Prasannakumar et al., 2012). Despite these limitations, the balance between the model's simplicity and reliability, along with the possibility of improvement through modern spatial data, makes RUSLE a suitable and effective choice for contemporary studies on erosion risk assessment and soil conservation planning (Borrelli et al., 2017; Rejani et al., 2022).

This study aims to quantify and map soil loss rates in the Upper Bouselam watershed (UBW) by applying the RUSLE Equation within a Geographic Information System (GIS) environment. This integrated approach combines multiple geo-environmental parameters such as rainfall erosivity (R), soil erodibility (K), slope

gradient (*LS*), vegetation cover (*C*), and conservation practices (*P*); to produce spatially explicit soil loss maps. These maps identify erosion hotspots and provide insights into the relative influence of different controlling factors.

Recent research has increasingly highlighted the value of RUSLE-based modelling for understanding soil erosion processes in mountainous and semi-arid environments. For example, [Prasannakumar et al. \(2012\)](#) demonstrated how the integration of RUSLE with GIS can effectively capture the influence of slope gradients, vegetation cover and rainfall on erosion patterns in a forested watershed in Kerala, revealing clear erosion hotspots and underscoring the utility of high-resolution spatial mapping for land-use planning. In a similar context, [Thomas et al. \(2012\)](#) coupled RUSLE with a transport-limited sediment delivery model to evaluate both erosion and deposition dynamics in the Western Ghats, showing that only a fraction of the gross soil loss is ultimately exported and emphasizing the role of human activities in shaping sediment transport. More recently, [Mi et al. \(2025\)](#) combined the RUSLE–SDR approach with geographically weighted regression and path analysis to investigate erosion behaviour in Longnan City, illustrating how vegetation, slope and precipitation interact across different environmental thresholds to control erosion intensity. RUSLE applications in other mountain and semi-arid regions further confirm these trends. In the Gorgol basin, topography was shown to dominate erosion risk under current and projected climate conditions ([Alioune et al., 2025](#)), while studies in the Cheliff Basin of Algeria have demonstrated how land use, soil characteristics and aridity collectively influence soil-loss patterns ([Zerouali et al., 2025](#)). Comparable findings have been reported in the High Atlas Mountains of Morocco, where nearly 40% of the basin exhibits high to very high erosion susceptibility ([Ait Haddou et al., 2024](#)), and in the Ethiopian highlands, where long-term monitoring has linked erosion dynamics to changes in land cover ([Guche et al., 2024](#)).

Taken together, these studies highlight both the robustness of RUSLE for quantifying soil loss in complex terrain and the pronounced spatial and temporal variability that characterizes erosion in such settings, calling for context-specific model calibration. Building on this body of work, the present study applies RUSLE to (your study area), using updated climatic, soil and topographic datasets to generate a detailed erosion-risk assessment. This approach not only aligns with established methodological advances but also addresses a critical gap in the literature, namely, (insert novelty, e.g., “the combined influence of steep slopes and semi-arid Mediterranean conditions under ongoing land-use change”), which remains insufficiently explored in the region.

Recent studies have highlighted the importance of integrating the RUSLE model with advanced geospatial techniques, such as remote sensing and high-resolution digital elevation models, to improve the representation of soil erosion dynamics in semi-arid mountainous areas. [Hateffard et al. \(2021\)](#) reported that combining RUSLE with advanced topographic analysis allows for a more accurate understanding of the spatial variations in erosion intensity on steep slopes. Similarly, [Gezici et al. \(2025\)](#) demonstrated that integrating the model with future climate scenarios enhances the capacity to assess erosion development under climate change. In North Africa, [Sahli et al. \(2019\)](#) and [Ait Haddou et al. \(2024\)](#) showed

the effectiveness of remote sensing in improving the accuracy of RUSLE factors in degraded mountainous environments.

By coupling the model with advanced geospatial techniques, this research contributes to a more detailed understanding of erosion dynamics in mountainous semi-arid regions. The findings offer a scientific foundation for designing targeted soil conservation and sustainable land-use strategies aimed at reducing erosion and safeguarding agricultural productivity in northern Algeria. Furthermore, the methodological framework proposed here demonstrates the broader applicability of combining empirical erosion modeling and remote sensing (RS) for data-limited environments, particularly across the MENA region.

2 Study area

The Soummam watershed ranks among the largest hydrological basins in Algeria, encompassing an area of approximately 9,125 km², which accounts for nearly 19% of the total surface of the broader Algiers–Hodna–Soummam (AHS) Mega-basin. The Soummam drainage network is composed of nine major tributaries, among which Wady Boussellam constitutes the main contributor. This river stretches for about 150 km and drains a surface area of 5,010 km². Its catchment is subdivided into four sub-basins: UBW (C/15-06, S/1,785 km²), Middle Boussellam (C/15-07, S/1,234 km²), El Main (C/15-08, S/930 km²), and Lower Boussellam (C/15-09, S/1,061 km²). In this classification, C represents the sub-basin code assigned by the Agence des Bassins Hydrographiques (ABH), and S denotes the corresponding surface area ([Figure 1a](#)).

This study focuses on the Upper Boussellam Watershed (UBW), which spans approximately 1,785 km², accounting for nearly 35% of the total Boussellam catchment area. Designated under the ABH code 15–06, the watershed extends longitudinally for about 65 km ([Figure 1b](#)). As illustrated by the DEM ([Figure 1c](#)), the basin predominantly consists of an extensive plain, bordered by several notable highlands: to the north by Jebel Medjounes, Jebel Aïssel, Jebel Megris, and Jebel Matrona; to the east by Kef Boudjemline, Jebel Merouane, Jebel Youssef, and Jebel Sekrine; and to the south by Jebel Hassane, Jebel Sattor, and Jebel Boutaleb.

The climate within the UBW varies from semi-arid in the central and southern regions to humid in the northern parts. Winters are generally mild and relatively wet, while summers are hot and dry. The rainy season typically extends from September to May, representing the transitional period between the humid and arid climatic phases. The precipitation shows pronounced year-to-year variability, with annual totals typically falling between 300 and 500 mm and averaging roughly 449 mm/year ([Table 1](#)). Mean annual temperature is around 16.65 °C, while seasonal values range from approximately –3 °C in winter to nearly 38 °C in summer ([Table 2](#)).

Moreover, the precipitation isohyet maps produced by the National Agency for Water Resources indicate that the basin lies within a zone of pronounced spatial and temporal rainfall variability in eastern Algeria. This climatic heterogeneity plays a key role in shaping both hydrological dynamics and erosion processes in the region, ([Hamed et al., 2017](#); [Hamad et al., 2021](#); [Benmarce et al., 2023](#); [Hamed et al., 2024](#); [Ncibi et al., 2022](#); [Ncibi et al., 2023](#)).

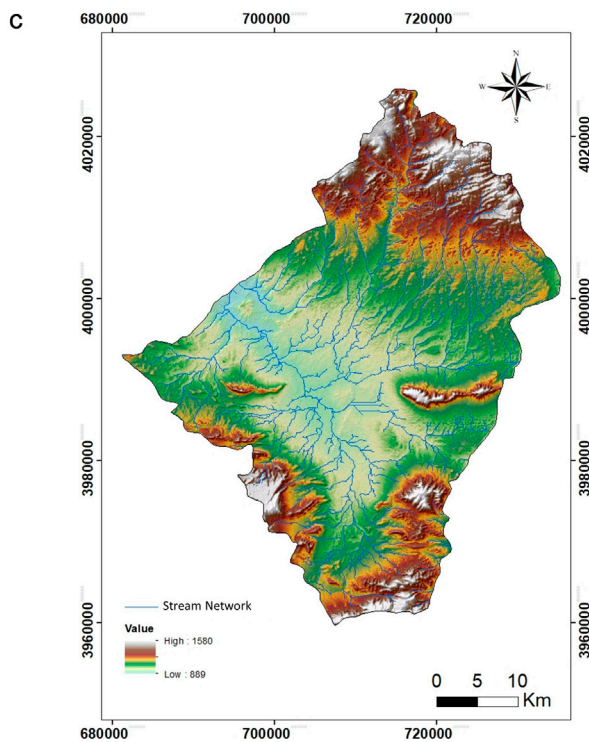
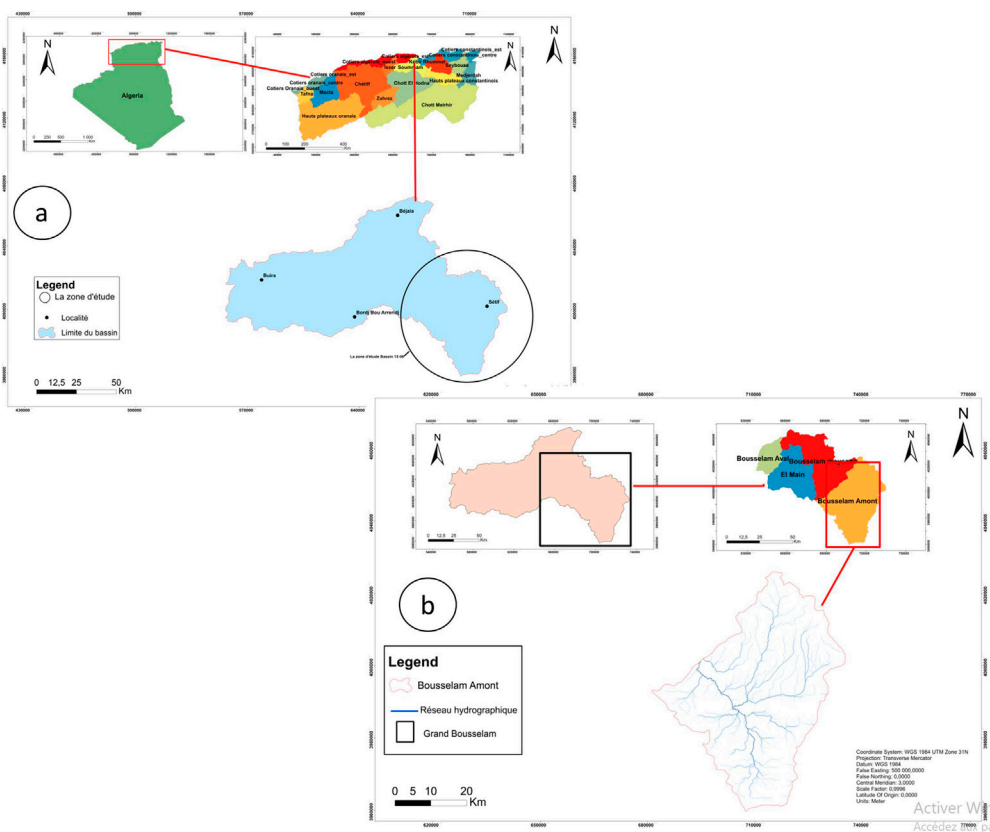


FIGURE 1
(a) Major watersheds of Algeria. **(b)** Location of the Upper Bousselam sub-watershed. **(c)** Digital Elevation Model (DEM) of the UBW.

TABLE 1 Interannual mean monthly precipitation (in mm).

Station	Jan	Feb	Mar	Ap	Ma	Ju	Jul	Au	Sep	Oct	Nov	Dec	P ann
Sétif	46.54	39.29	43.5	45.79	46.45	19.04	7.91	20.62	40.5	40.04	53.5	52.12	455.33
Bougaa	58.91	46.41	52.45	53.54	52.45	22.54	7.96	23.71	47.79	48.83	66.75	57.79	539.16
Ain kbira	58.5	47.75	55.5	54.71	56.75	24.66	8.91	27.21	49.29	51.62	70.21	60.37	565.5
Eulma	47.95	39.58	45.5	47.54	48.2&	20.37	8.12	21.62	42.12	40.91	54.79	53.79	470.54
Ain oulmen	42.71	36.33	42.875	49.33	48.54	20.21	7.62	19.91	41.25	37.95	44.29	46.87	437.91
Ain azel	41.29	34.5	41.87	46.62	42.62	17.87	6.79	18.33	38.83	34.87	42.75	46.45	412.83
Ain zada	46.45	39.91	42.83	46.37	48	20.08	7.71	20.87	41.75	40.87	54.71	51.75	461.33
Bir kasdeli	46.45	39.91	42.83	46.37	48	20.08	7.71	20.87	41.75	40.87	54.71	51.75	461.33
Boutaleb	40.58	31.70	37.12	41.25	38.08	15.58	6.5	15.5	36.66	33.21	38.95	43.87	379.04
Hamem sou	42.25	34.37	37.5	43.58	42.25	18.37	7.83	16.25	39.87	36.5	41.87	45.21	405.87
Ain abassa	59	47.58	55.04	55.21	55.54	23.58	8.66	27.12	49.87	50.66	68.87	58.83	560
Guedjel	46.54	39.29	43.5	45.79	46.45	19.04	7.91	20.62	40.5	40.04	53.5	52.12	455.33
Mezlog	46.54	39.29	43.5	45.79	46.45	19.04	7.91	20.62	40.5	40.04	53.5	52.12	455.33
Elghdir	45	39.91	42.83	53.58	54.21	23	8.83	21.58	43.91	43.91	51.5	46.79	475.08
Ain lehdjar	41.29	34.5	41.87	46.625	42.62	17.87	6.79	18.33	38.83	34.87	42.75	46.45	412.83

TABLE 2 Interannual mean monthly temperatures (°C).

Station	T(C°)	J	F	M	A	M	J	J	A	S	O	N	D	Ann
Sétif	Tmax	16.98	18.28	22.66	26.90	31.334	35.92	38.13	37.532	33.66	28.40	21.64	17.47	38.36
	Tmin	-3.56	-3.49	-2.36	0.44	4.45	8.64	12.53	13.72	9.80	5.54	0.38	-2.36	-4.69
	Tmoy	6.71	7.39	10.15	13.67	17.89	22.28	25.33	25.63	21.73	16.97	11.01	7.55	16.83
Ain- zada	Tmax	16.68	17.92	22.46	26.52	31.02	35.66	37.89	37.40	33.31	28.19	21.33	17.01	38.19
	Tmin	-3.96	-3.85	-2.98	0.27	3.66	8.13	12.07	13.05	9.20	4.86	-0.05	-2.99	-5.22
	Tmoy	6.35	7.03	9.73	13.39	17.34	21.89	24.98	25.22	21.25	16.53	10.64	7.009	16.48

From a hydrological standpoint, the sub-basin is drained by the Wady Boussellam, which forms the main watercourse and receives inflows from several tributaries, including Wady Malah (Ain Arnat), Wady Malah (Ksar El Abtal), Wady Fermatou, Wady Guellal, Wady Tixter, and Wady Ftaïssa. Together, these streams contribute an estimated annual discharge of approximately 50 M hm³/year (Khemmal et al., 2025).

The topography of the basin is characterized by moderate to steep slopes, with elevations ranging between 900 and 1,600 m. The highest altitudes are found in the mountainous regions to the north and south, while the central portion of the basin; extending toward

the Ain Zada Dam; is distinguished by gentler relief and lower elevations around 900 m (Rouibah and Belabbas, 2022).

In terms of geology, the UBW is largely covered by Quaternary deposits, particularly in its northern sector, where Eocene formations with intermediate materials are also present, along with flysch sequences in the upstream zones (Hadiji et al., 2016). The central area features Eocene parautochthonous, autochthonous, and allochthonous units, whereas Mio-Pliocene formations occur in the northwestern part. Quaternary accumulations are also found along the piedmont zones. In the southwestern sector, the substratum is mainly composed of Hodna parautochthonous and

autochthonous units, interspersed with Triassic exotic outcrops (Figure 2) (Benmarce et al., 2024).

Extensive carbonate formations outcrop throughout the region, consisting primarily of limestone, marl, clay, sandstone, dolomite, and Quaternary crusts, often associated with tufa deposits (Mebraska and Boufekane, 2020).

3 Materials and methods

3.1 Data sources

The implementation of the RUSLE model required the integration of multiple geospatial, climatic, and soil-related datasets. These include a DEM, precipitation measurements, soil property data, and multispectral satellite imagery. All input layers were standardized to ensure spatial consistency during GIS-based processing and to enable reliable computation of the RUSLE factors (Romshoo et al., 2021) (Table 3).

3.1.1 Digital elevation model (DEM)

Topographic information was derived from a 12.5-m ALOS PALSAR DEM obtained through the U.S. Geological Survey. The DEM served as the foundation for calculating slope and flow-accumulation surfaces, which were subsequently used to derive the LS factor. Prior to analysis, the DEM was resampled to a uniform 10-m resolution to match the other RUSLE layers. Standard preprocessing steps included sink filling and removal of spurious artifacts to minimize topographic noise.

3.1.2 Rainfall data

Rainfall observations from 15 stations within and near the watershed were sourced from the WaterBalance platform. These point data were interpolated into a continuous rainfall erosivity surface using Inverse Distance Weighting (IDW). To maintain spatial consistency, the interpolated *R*-factor raster was generated directly at the target 10-m resolution and aligned with the common projection. Uncertainty in the *R* layer primarily stems from the spatial distribution of stations, interpolation method, and temporal variability of rainfall; these aspects were evaluated through cross-validation of IDW performance.

3.1.3 Soil data

Soil characteristics were compiled from 1:50,000 geological maps, complemented by laboratory analyses of field-collected samples. Particle-size distribution and soil permeability were used to compute the *K* factor. All soil polygons were converted to raster format and resampled to 10 m to harmonize with the other inputs. Potential uncertainties in the *K* factor arise from scale discrepancies in the soil maps and from laboratory-based estimation of texture and permeability; these were minimized through field verification at representative locations.

3.1.4 Cover–management data

Vegetation cover was derived from Sentinel-2A imagery (10-m resolution) accessed via the Copernicus DataSpace platform. After atmospheric correction and cloud masking, NDVI was computed

and subsequently transformed into *C*-factor values following established empirical relationships. Sentinel-2A data were selected to ensure compatibility with the target spatial resolution, reducing resampling-related uncertainty.

3.2 Methodology

The evaluation of soil erosion dynamics in the UBW was conducted through an integrated geospatial modeling framework that combines GIS and RS techniques. This integrated approach enabled the spatial implementation of the RUSLE Equation. This model estimates the average annual soil loss by representing the landscape as a grid of raster cells, thus facilitating a continuous spatial assessment of erosion intensity across diverse terrain conditions.

The methodological workflow involved identifying, mapping, and quantifying the main biophysical and anthropogenic factors influencing soil erosion. Each parameter; namely, rainfall erosivity (*R*), soil erodibility (*K*), topographic factor (*LS*), vegetation cover and management (*C*), and support practice (*P*); was computed as an independent raster layer with a spatial resolution of 10 m. All datasets were harmonized under the WGS 1984-UTM-31N coordinate system to ensure spatial consistency. The integration of these layers using raster-based multiplication produced a composite erosion potential map expressing the spatial distribution of soil loss across the watershed.

The RUSLE model is mathematically expressed as Equation 1:

$$A = R \times K \times LS \times C \times P \quad (1)$$

where: *A* = average annual soil loss (t·ha⁻¹·yr⁻¹),
R = rainfall erosivity factor (MJ·mm·ha⁻¹·h⁻¹·yr⁻¹),
K = soil erodibility factor (t·ha·h/ha·MJ·mm),
LS = topographic factor (slope length and steepness),
C = vegetation cover and management factor (dimensionless), and
P = support practice factor (dimensionless), representing the soil conservation measures.

The study workflow comprised five principal stages: i: *Data Collection and Compilation*: Long-term precipitation data (2000–2023) from 14 stations, Sentinel-2A imagery, field-collected soil samples, and a 12.5 m ALOS PALSAR DEM were compiled. ii: *Data Preprocessing*: All spatial datasets were georeferenced to the WGS 1984/UTM 31N system and resampled to a 10 m resolution. Preprocessing included atmospheric correction, cloud masking, NDVI computation, and data standardization. iii: *Derivation of RUSLE Parameters*: Each factor (*R*, *K*, *LS*, *C*, *P*) was computed individually using empirical or physically based formulations, with GIS tools applied for spatial analysis and rasterization. iv: *Integration and Spatial Modeling*: The five factor layers were integrated in GIS using raster algebra according to the RUSLE equation to produce a spatially explicit soil loss map (t·ha⁻¹·yr⁻¹). v: *Classification and Validation*: Computed soil loss values were reclassified into five erosion levels: very low, low, moderate, high, and very high. Validation involved field verification, comparison with land-use data, and consistency checks against known erosion-prone zones.

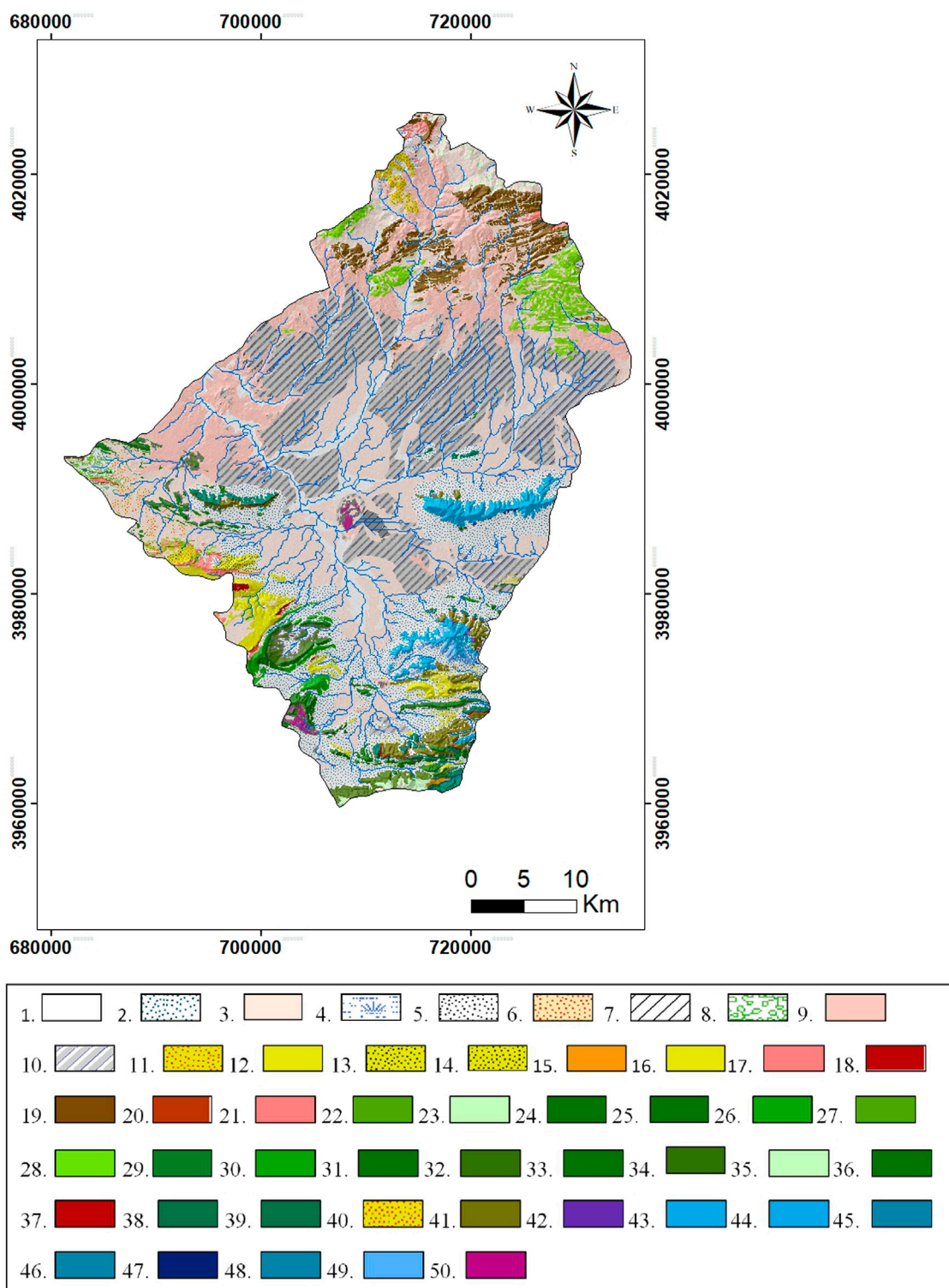


FIGURE 2

Geological map of the upper bousselam sub-watershed. 1. A: Recent alluvium. 2. Polygenic glacia covering the reliefs. 3. Q: Arable lands, slope deposits, ancient alluvium, and undifferentiated Quaternary formations. 4. Quaternary: Blocky scree with marly matrix, showing detachment niches. 5. Quaternary: Dunes. 6. Quaternary: Ider terrains with calcareous crusts, isolated or interbedded within Mio-Pliocene deposits. 7. Sebkhia soils. 8. Topsoil and marly eluvium 9. mp: Continental Mio-Pliocene - reddish sandy clays and poorly cemented conglomerates. 10. Probable Villafranchian:

(Continued)

FIGURE 2 (Continued)

Lacustrine limestones, crusted soils, and fluvial gravels. 11. Lower Miocene: Red clays, sands, and conglomerates. 12. Miocene: Conglomerates, oyster-bearing marls, and sandy limestones. 13. Lower Miocene Reddish marls and calcareous microbreccias with pectinids. 14. Marine Miocene: Calcareous sandstones with Melobesiae and marks. 15. Oligocene: Conglomerates, gravellites, limestones, and red sandstones. 16. Eocene: Massive detrital limestones with silicified Thersites. 17. Middle to Upper Eocene: Black, brown, or gray marls with yellow beds and nodules. 18. Upper Lutetian: Gypsiferous clays and limestones. 19. et-5s: Ypresian to Lower Lutetian-marly, schistose limestones with white patina, black fracture, and black flints; Globigerina facies. 20. Ypresian-Lower Lutetian: Phosphatic white limestones with black flints and abundant debris. 21. Danian-Paleocene to Ypresian: Blackish marls. 22. Maastrichtian-Danian-Montian: Gray marls with subordinate limestones. 23. E3-C6: Maastrichtian to Paleocene- undifferentiated black marls, sometimes with yellow nodules in the eastern two-thirds of the sheet. 24. Upper Senonian: Marls and crystalline limestones with oyster debris. 25. Upper Senonian: Yellowish biosparites and shell beds with Orbitoides. 26. Upper Senonian: Pebbly marls, marly limestones, and sometimes sandy limestones with Orbitoides. 27. C5-6: Upper Campanian and Lower Maastrichtian-dark marly formations with abundant yellow nodules. 28. C6C: Upper Campanian and Maastrichtian- lenticular and micritic limestones in the north, becoming thicker, well-bedded, and rich in shell debris near Djebel Medjoun. 29. C4-5: Upper Santonian to Campanian - well-bedded marly limestones with oyster debris near Djebel Anini. 30. C3-4: Coniacian-Santonian-gray marls alternating with gray marly limestones north of Djebel Anini. 31. Upper Coniacian-Santonian: Gray marls around Koudiat Della. 32. Upper Cenomanian and Turonian: Dolomites and limestones with flints or milioids. 33. Upper Cenomanian and Turonian: Fine or gravelly limestones with Miliolidae. 34. Vraconian-Lower Cenomanian: Marls and marly limestones. 35. Albian: Argillaceous and sandy limestones with dolomitic beds and quartzose marly sandstones. 36. Late Aptian-Albian: Clays, marls, sandstones, and biosparites with Melbesio. 37. Marly yellow Aptian. 38. Aptian: Limestones with Orbitolites and dolomites. 39. Aptian: Limestones with Orbitolines and Ovalveolina reicheli in the upper beds. 40. Coarse sandstone bars with clayey intercalations. 41. Barremian: Massive limestones, dolomites, marls, and sandstones. 42. Neocomia: Sandstones, pelites, and marls with ammonites and brachiopods. 43. Upper Jurassic: Limestones with Clypeina jurassica. 44. Upper Jurassic: Dolomitic facies. 45. Middle Jurassic: Variegated limestones with Pygopes. 46. Jurassic-Cretaceous transition: Algal or Calpionellid facies. 47. Dolomitic Lias. 48. Upper Lias: Marls and marly limestones. 49. Dogger: Bedded marly limestones. 50. Exotic Triassic: Clays, crushed gypsum, and massive calcareous dolomitic rocks.

TABLE 3 Data information used in RUSLE model.

Data	Data type	Spatial resolution/Scale	Source	Factor
DEM	Raster (GeoTIFF)	12.5 m	USGS EarthExplorer	LS,P
Rainfall data	Tabular (XLS)	Point measurements (15 stations)	WaterBalance platform	R
Soil data	Vector + Tabular (Shapefile + XLS)	1:50,000	Geological maps; laboratory and field test	K
Satellite imagery	Raster (GeoTIFF)	10 m	Copernicus DataSpace	C

3.2.1 Rainfall erosivity factor (R)

The rainfall erosivity factor (R) expresses the potential kinetic energy of rainfall to detach and transport soil particles. Among the parameters of the RUSLE model, R exerts one of the strongest influences on erosion rates (Yin et al., 2017). In its original formulation, R is defined as the product of the total kinetic energy of rainfall (E) and the maximum 30 min rainfall intensity (I_{30}). However, due to the lack of high-temporal-resolution pluviographic data for the study area, this direct computation was not feasible.

To address this limitation, empirical relationships suited to regions with incomplete rainfall data were adopted. Among several fundamental works (Kalman, 1967; Arnoldus, 1980), the Rango and Arnoldus (1987) formulation was selected, as it has been widely validated in North African and Mediterranean contexts. The relationship is expressed as Equation 2:

$$R = 1.74 \times \left(\log \sum \frac{P_i^2}{P} \right) + 1.29 \quad (2)$$

where R is the rainfall erosivity factor ($\text{MJ}\cdot\text{mm}\cdot\text{ha}^{-1}\cdot\text{h}^{-1}\cdot\text{yr}^{-1}$), P_i is the monthly rainfall (mm), and P represents the annual precipitation (mm).

For this study, rainfall data from 14 meteorological stations located within and around the watershed were analyzed over a

24-year period (2000–2023). Computed R values were spatially interpolated using GIS-based geostatistical techniques (Inverse Distance Weighting, IDW) to generate a continuous rainfall erosivity surface for the entire basin.

3.2.2 Vegetation cover and management factor (C)

The C factor quantifies the mitigating effect of land cover on soil erosion by comparing soil loss under actual vegetation conditions to that from bare soil (Chang-guang et al., 2012). Values of C close to zero indicate surfaces that are well-protected by vegetation, while values approaching one correspond to bare or sparsely vegetated areas (Wischmeier and Smith, 1978; Roose, 1977; Roose, 1994).

Vegetation reduces erosion through multiple mechanisms: intercepting raindrops, dissipating their kinetic energy, improving soil structure and infiltration, and slowing surface runoff. In this study, the Normalized Difference Vegetation Index (NDVI) was derived from Sentinel-2A imagery (10 m spatial resolution) to represent the spatial variability of vegetation cover. The empirical relationship between NDVI and the C factor was established using the regression proposed by Van der Knijff et al. (1999), Equation 3:

$$C = e^{\left[-\alpha \times \left(\frac{\text{NDVI}}{\beta - \text{NDVI}} \right) \right]} \quad (3)$$

where the empirical coefficients $\alpha = 2$ and $\beta = 1$ control the curvature of the NDVI– C relationship. This formulation allows for a gradual and realistic transition of C values from dense vegetation ($C \approx 0$) to bare soil ($C \approx 1$), accurately reflecting the land-cover heterogeneity of the UBW.

3.2.3 Support practice factor (P)

The P factor reflects the effectiveness of human interventions designed to minimize surface runoff and reduce soil erosion. It represents the ratio between soil loss under a specific conservation practice and that under conventional upslope cultivation (Foster et al., 1997). Typical practices include terracing, contour farming, strip cropping, and vegetative barriers, all of which help decrease runoff velocity and enhance soil stability (Shin, 1999). P values range from 0 to 1, where values close to one denote areas lacking conservation practices, while values near 0 correspond to well-managed or terraced zones. Based on land-use type, slope gradient, and local agricultural practices, P values were assigned from published literature and adapted to the geomorphological conditions of the study area (Foster et al., 2003).

3.2.4 Topographic factor (LS)

The topographic factor (LS) accounts for the combined influence of slope length (L) and slope steepness (S) on erosion processes (Efthimiou et al., 2020). These parameters determine the accumulation and velocity of overland flow, directly influencing the soil's detachment and transport capacity (Stone and Hilborn, 2000).

The LS factor was derived from a 12.5 m resolution DEM obtained from the ALOS PALSAR platform. Terrain attributes such as slope and flow accumulation were computed in GIS using hydrological analysis tools (Table 1). The LS factor was then calculated according to the Equation 4, Moore and Burch (1986):

$$LS = \left(\frac{FA \times r}{22.13} \right)^{0.4} \times \left(\frac{\sin(\text{slope} \times 0.01745)}{0.0896} \right)^{1.4} \quad (4)$$

where FA is the flow accumulation (number of contributing cells), r is the cell resolution (12.5 m), and slope is expressed in degrees. This approach provides a detailed spatial quantification of topographic controls on erosion potential (Michalopoulou et al., 2022).

3.2.5 Soil erodibility factor (K)

The K factor measures the inherent vulnerability of soil to detachment and transport by rainfall and surface runoff (Römkens, et al., 1997). It reflects the combined effects of soil texture, organic matter content, structure, and permeability; parameters that determine the soil's resistance to erosive forces (Wischmeier et al., 1971).

In this study, K was estimated using the Equation 5, Wischmeier and Smith (1978):

$$K = \frac{2.1 \times 10^{-4} M^{1.14} (12 - \alpha) + (b - 2) + 2.5(c - 3)}{100} \quad (5)$$

where:

- M = (% silt + % fine sand) \times (100 – % clay),
- α = organic matter content (%),
- b = permeability class (1–6), and
- c = soil structure code (1–4).

A field campaign was undertaken to collect approximately 20 representative soil samples across various lithological and land-use units of the watershed. Laboratory analyses determined granulometric composition and organic matter content, while field assessments characterized structure and permeability classes. The derived K values were spatially interpolated to produce a continuous erodibility surface layer, which was integrated into the RUSLE model.

The complete sequence of operations; from data acquisition to the generation of the final soil erosion map is represented in the methodological flowchart (Figure 3).

4 Results and discussion

The results obtained from applying the RUSLE model to the UBW reveal complex, spatially heterogeneous erosion dynamics; shaped by the combined influence of rainfall, soil properties, topography, vegetation cover, and land management. Below I discuss how each RUSLE factor contributes to the observed patterns, compare with findings from recent studies, and reflect on regional implications of the results.

4.1 Rainfall erosivity (R) and its role

Based on 24 years (2000–2023) of precipitation data from 14 stations, the spatial interpolation of R values produced an erosivity map (Figure 4a). R ranged from ~ 54 MJ·mm·ha⁻¹·h⁻¹·yr⁻¹ in the southern stations to ~ 73 MJ·mm·ha⁻¹·h⁻¹·yr⁻¹ in the northern highland zones. The highest erosivity class is concentrated in the northern portion of the basin, while lower values dominate the southern plains.

This north-south gradient (with higher R values in more elevated, wetter, and steeper areas) echoes the results of a recent Mediterranean-region RUSLE-GIS analysis, where rainfall intensity significantly governed erosion hotspots, especially when paired with slope and sparse vegetation cover (Fadl et al., 2025).

Additionally, a very recent RUSLE-based study from northeastern Turkey showed that steep topography combined with spatially variable rainfall patterns led to high erosion risk zones, even when average basin-wide values suggested moderate susceptibility (Gezici et al., 2025).

These comparisons support the idea that in regions like UBW (with complex topography and variable precipitation) the R factor can act as a primary driver of erosion potential, rather than just a background forcing parameter.

4.2 Vegetation cover and land management (C and P factors)

Our NDVI-derived C factor map (Figures 4b,c) indicates widespread bare or sparsely vegetated surfaces covering $\sim 63\%$ of the watershed. Areas with moderate vegetation cover (seasonal crops) represent $\sim 27\%$, while denser vegetation (forest, shrublands) covers only $\sim 9.5\%$, mainly along Wadi Boussem and in mountainous pockets. Thus, protective land cover is localized and discontinuous.

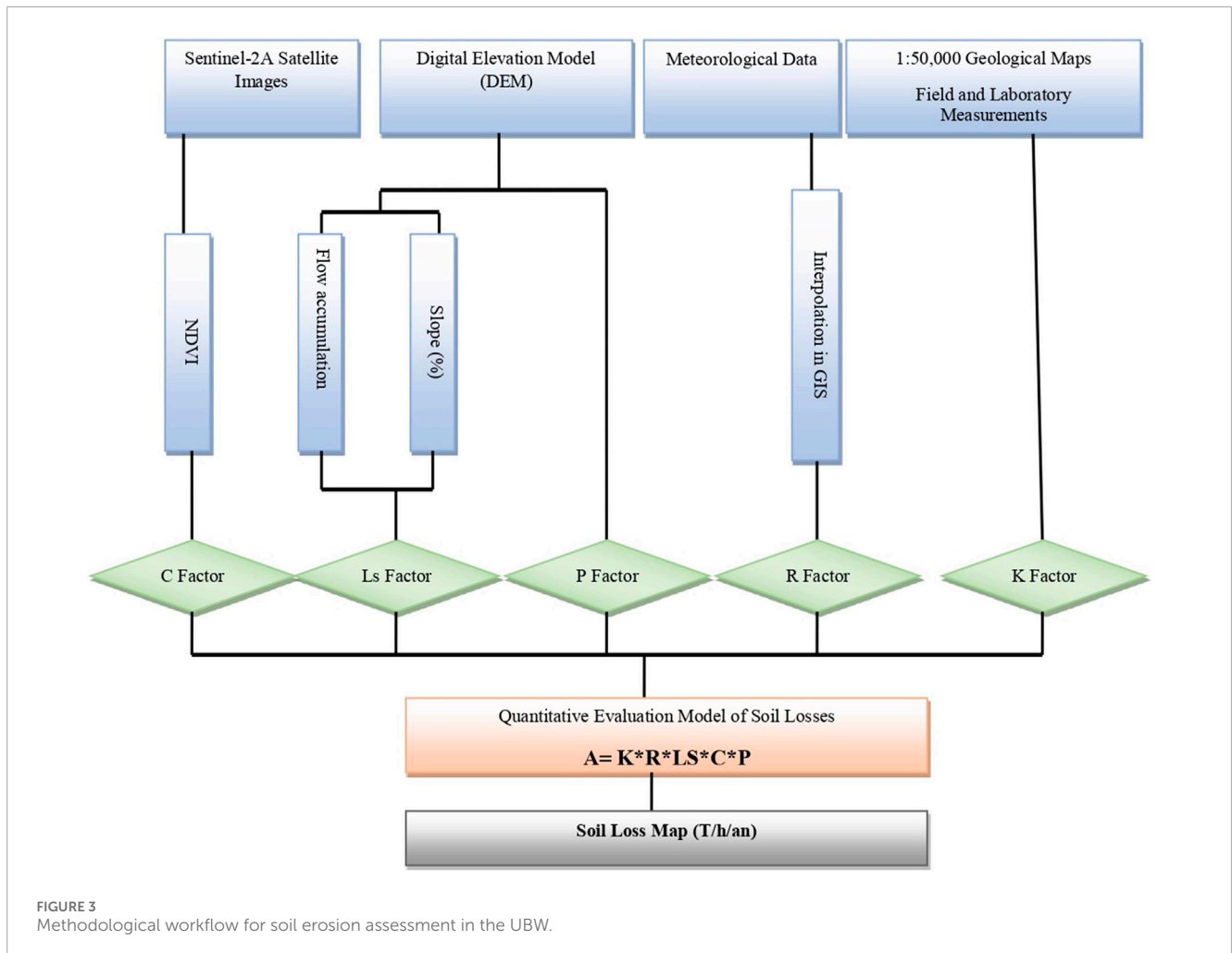


FIGURE 3
Methodological workflow for soil erosion assessment in the UBW.

This pattern concurs with broader regional findings. For example, a recent study applying RUSLE–GIS in a Mediterranean plain under similar semi-arid conditions identified poor vegetation cover and land-use fragmentation as leading contributors to erosion risk (Fadl et al., 2025). Moreover, in steep, mountainous or semi-arid watersheds where vegetation is patchy, even high rainfall erosivity does not always translate proportionally to high soil loss; this decoupling was documented in a humid-mountain watershed study, where dense vegetation sometimes failed to prevent severe erosion under extreme rainfall and steep slopes (Hag Husein et al., 2024). Thus, in UBW, the scarcity and discontinuity of protective cover likely amplify soil vulnerability. The limited effectiveness of conservation practices (*P* factor) on steep slopes further increases the risk, especially in areas where *P* values approach (Figure 4d).

4.3 Topography (*LS* factor) and soil erodibility (*K* factor)

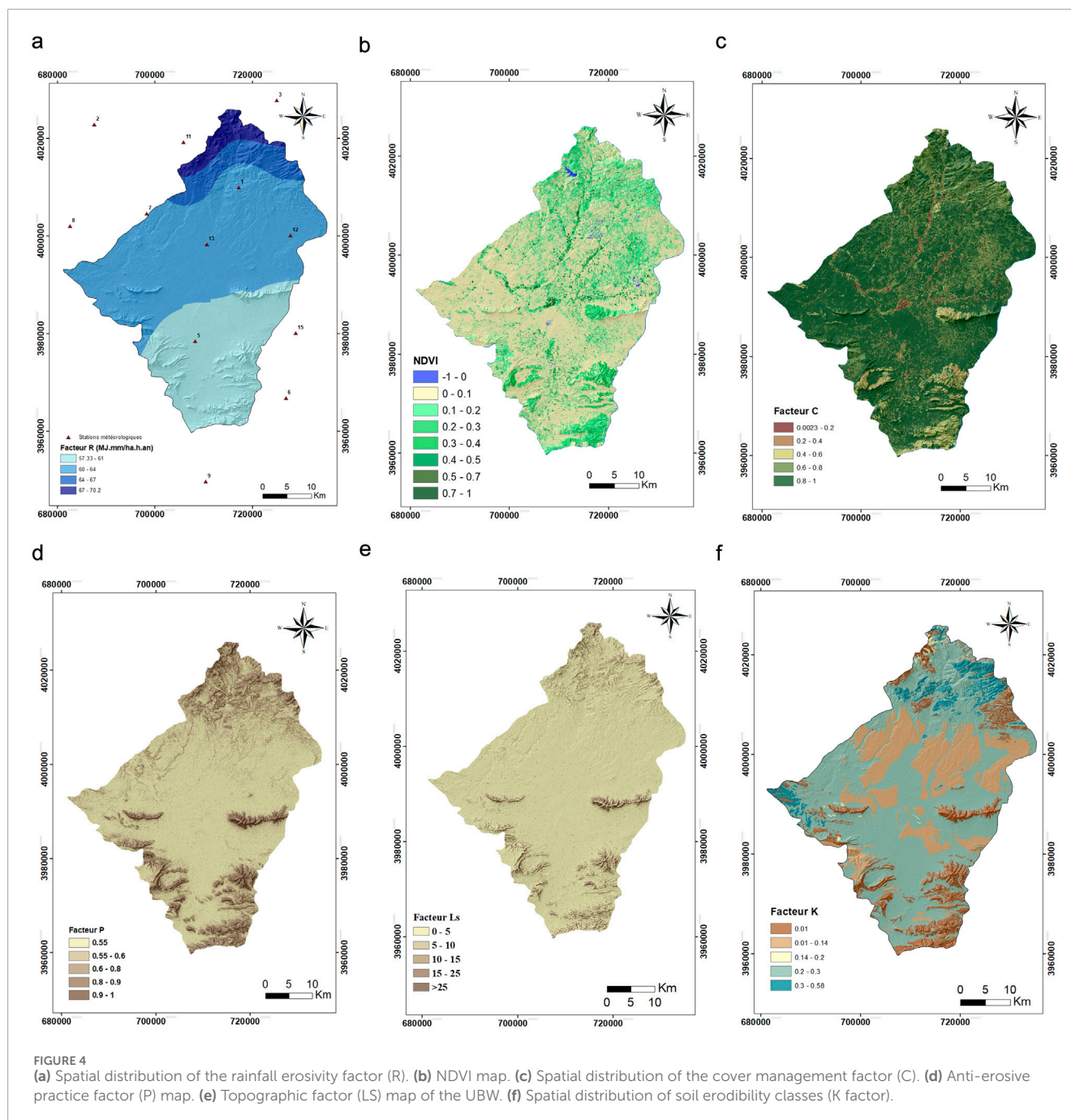
The *LS* factor derived from DEM shows a wide range, from near 0 on gentle plains to over 25 in steep mountainous zones (Figure 4e). Flat and gently undulating areas ($LS = 0\text{--}5$) dominate ~87.4% of the basin; indicating limited slope-driven erosion in the

majority of the landscape. However, steeper piedmont and mountainous zones (though covering a smaller area) exhibit much higher *LS* values, and thus disproportionately higher erosion risk.

This spatial topography–erosion relationship is well-aligned with findings from other RUSLE-based regional studies. In the northeastern Turkey analysis, steep topographic sectors were identified as major erosion hotspots, reinforcing the importance of *LS* in modulating overall soil loss (Gezici et al., 2025).

Regarding soil erodibility (*K*), our results show strong variability (0.01–0.4), reflecting heterogeneity in texture, structure, organic matter content, and soil cohesion (Figure 4f). Soils with high silt content and low organic matter (often found in plains and glacial deposits) present higher erodibility; whereas rocky outcrops and cohesive soils (limestones, compact deposits) show low erodibility. These patterns are consistent with soil-erosion dynamics reported in semi-arid to Mediterranean environments, where erodibility strongly correlates with soil texture and organic matter content (Charef et al., 2025).

The designation of each erosion-related factor, including the defined categories, their numerical thresholds, and the proportion of watershed area belonging to each class, is summarized in Tables 4–9.



4.4 Spatial distribution of soil loss and erosion hotspots

Combining all factors in the RUSLE equation produced spatial soil loss estimates ranging from ~ 0 to $>33 \text{ t ha}^{-1}\cdot\text{yr}^{-1}$ (Figure 5). Roughly 70% of UBW is characterized by low erosion rates ($<6 \text{ t ha}^{-1}\cdot\text{yr}^{-1}$), typically in flat plains with some vegetation cover. Moderate ($5\text{--}15 \text{ t ha}^{-1}\cdot\text{yr}^{-1}$) and high ($>15 \text{ t ha}^{-1}\cdot\text{yr}^{-1}$) erosion zones are concentrated on steep slopes, particularly in mountainous and piedmont zones where vegetation is sparse, soils are erodible, and conservation practices are minimal (Figure 6).

This spatial heterogeneity matches patterns found in other recent RUSLE-GIS studies across Mediterranean and semi-arid basins, where erosion hotspots are often localized in steep, sparsely vegetated landscapes rather than uniformly distributed (Fadl et al., 2025).

Furthermore, the marked contrast between plains and hillslopes underscores the importance of terrain and land cover interplay; a conclusion supported by studies showing that even in humid mountain regions, steep slopes greatly exacerbate erosion despite vegetation cover (Hag Husein et al., 2024).

TABLE 4 Values of the R factor Vs. the annual precipitation at the different stations.

Station	Longitude	Latitude	R factor	Precipitation
Setif	717191.55	4010060.49	62.2	455.33
Bougaa	687570.13	4022921.53	71.08	539.16
Ain kbira	724958.31	4027860.38	73.2	565.5
Eulma	742904.00	4004020.00	63.66	470.54
Ain oulmene	708228.07	3978512.75	60.07	437.91
Ain azel	726805.68	3966812.66	57.75	412.83
Ain zada	698273.83	4004640.71	62.76	461.33
Bir kasdeli	682603.84	4002113.44	62.76	461.33
Boutaleb	710362.644	3949676.728	54.34	379.04
Hamem sou	753343.095	3985155.396	56.8	405.87
Ain abassa	705867.71	4019282.93	72.71	560
Guedjel	727756.56	4000146.33	62.2	455.33
Mezloug	710606.144	3998338.155	62.2	455.33
Elghdir	671289.452	3974557.815	63.71	475.08
Ain lehdjar	728824.84	3980149.58	57.75	412.83

TABLE 5 Different classes of the C-factor.

Classe	C	Surface ha	Surface %
1	0.0023–0.2	3083.5	1.753904
2	0.2–0.4	3640.59	2.070779
3	0.4–0.6	10009.45	5.693406
4	0.6–0.8	47863.63	27.22498
5	0.8–1	111210.6	63.25692

TABLE 7 Classes of the LS factor.

Ls factor	Surface in ha	Percentage
0–5	153588.4	87.36242
5–10	11444.58	6.509775
10–15	5034.594	2.86372
15–20	2474.125	1.407304
>20	3264.344	1.856787

TABLE 6 Values of the P-Factor.

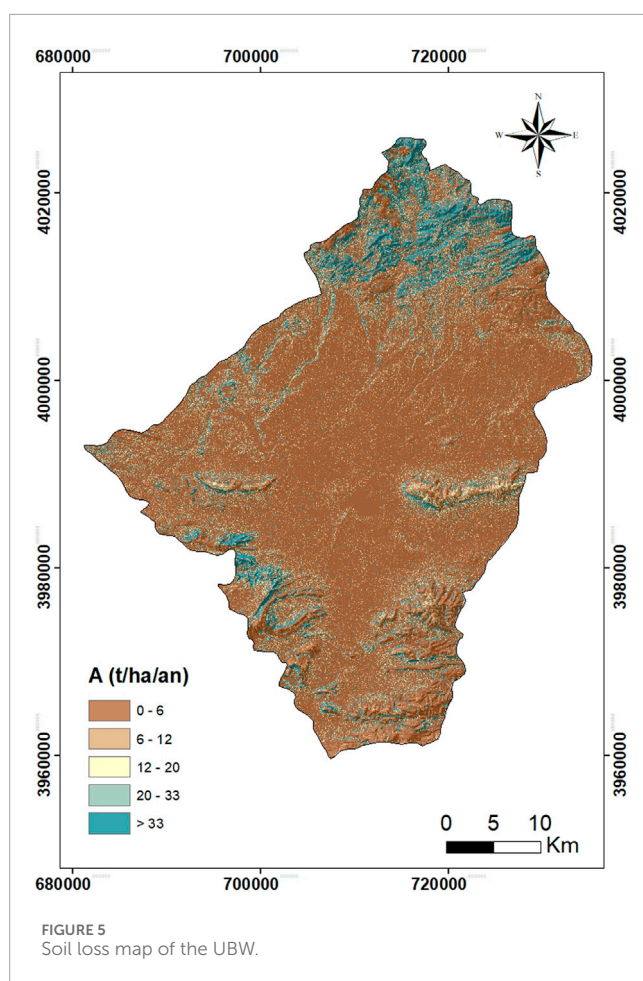
P Facteur	Superficie ha	Percentage
0.55	102909.5	58.53784
0.6	31779.47	18.07705
0.8	19354.39	11.00932
0.9	11982.64	6.816064
1	9773.994	5.559722

TABLE 8 Different classes of soil erodibility according to area.

Classe	K	Surface	Percentage %
1	0.01	29301.64	16.66712
2	0.01–0.14	38357	21.81791
3	0.14–0.20	796.44	0.453024
4	0.20–0.3	105519.4	60.02068
5	0.3–0.4	1830.59	1.041261

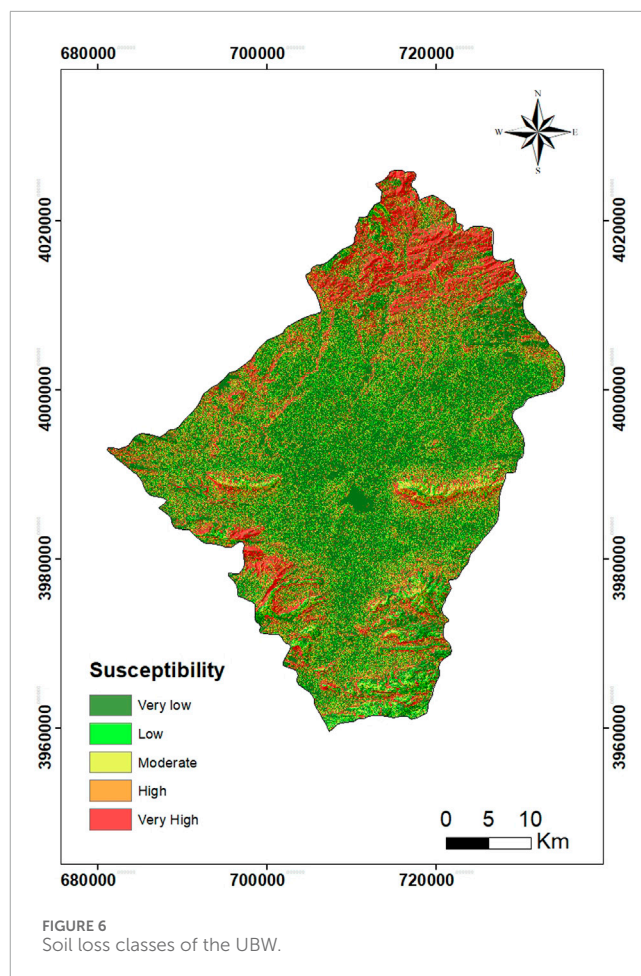
TABLE 9 The anti-erosive practice factor as a function of slope (Shin, 1999).

Slope %	P factor
0–7	0.55
7–11.3	0.6
11.3–17.6	0.8
17.6–26.8	0.9
>26.8	1



4.5 Implications, model strengths, and limitations

The congruence between our findings and those reported in recent literature confirms that the RUSLE–GIS approach remains a robust, practical tool for assessing soil erosion risk in semi-arid to Mediterranean watersheds, including UBW. Similar to a recent study in northeastern Turkey under changing climate, our results highlight how spatial heterogeneity (rather than average basin-wide metrics) best captures erosion risk distribution and helps target conservation efforts (Gezici et al., 2025). Nevertheless,



some limitations must be acknowledged. As earlier studies have pointed out (in Mediterranean contexts where RUSLE tends to overestimate actual soil loss), our model does not account for certain local processes such as gully erosion, sediment deposition, or land-use change dynamics. Moreover, given the fragmentation and low density of vegetation, small-scale land management practices or episodic extreme events may alter erosion patterns beyond what RUSLE predicts. Similar challenges were discussed in semi-arid Algerian basins where sparse data and heterogeneous land cover complicate direct comparisons with empirical measurements (Hammad et al., 2004).

4.6 Treatment of uncertainty

Although each RUSLE factor introduces its own sources of uncertainty, steps were taken to reduce and document them:

R factor: Uncertainties assessed from station density and IDW cross-validation.

K factor: Variability linked to soil map resolution and laboratory-derived texture measurements; mitigated through field checks.

LS factor: Sensitive to DEM accuracy; preprocessed to remove sinks and artifacts.

C factor: Dependent on seasonal NDVI fluctuations; addressed by selecting imagery from representative phenological periods.

P factor: Derived from slope classes; uncertainty linked to generalized assumptions regarding local conservation practices.

4.7 Limitations and future perspectives

While the RUSLE–GIS framework offers a practical means of examining erosion dynamics across the UBW, the results must be interpreted in light of several methodological constraints. A first limitation concerns the heterogeneous spatial resolution of the input datasets—namely the DEM, land-cover layers, and soil information—which may smooth or obscure small-scale features such as micro-relief variations, localized farming practices, or narrow erosion pathways. Moreover, the RUSLE model represents a simplified, steady-state view of erosion and does not explicitly capture transient or process-driven phenomena such as gully development, sediment deposition, channel bank retreat, or rapid land-use shifts. These omissions can lead to discrepancies between modelled soil loss and field conditions, particularly in highly dynamic parts of the basin. Parameter uncertainties also play a role: the interpolation of rainfall erosivity, the estimation of the C factor from NDVI, and the attribution of soil erodibility values all involve assumptions that could not be fully validated due to limited ground data. In addition, the temporal scope of the analysis reflects long-term averages and therefore does not account for the impact of short, intense storm events that often dominate sediment generation in semi-arid environments. Looking forward, future work would benefit from integrating higher-resolution datasets, expanding field-based sediment monitoring programmes, and combining RUSLE with physically based or sediment-delivery models. Such enhancements would improve the representation of local processes and strengthen the predictive capacity of erosion assessments under evolving climatic and land-use conditions.

4.8 Recommendations for conservation

The concentration of elevated erosion risk on steep slopes, highly erodible soils, and areas lacking sufficient vegetation highlights the urgent need for targeted soil and water conservation measures across the UBW. Drawing on both the present findings and evidence from comparable Mediterranean and semi-arid basins, several strategies emerge as particularly effective. Slope stabilization remains a priority, especially in sectors characterized by high *LS* values, where terracing, contour farming, and the installation of vegetative buffer strips have been shown to substantially reduce soil loss (Gezici et al., 2025). Increasing long-term vegetative cover through reforestation, assisted natural regeneration, and the protection of riparian corridors can further enhance soil cohesion and reduce runoff velocities; benefits consistently reported in recent RUSLE-based studies (Fadl et al., 2025). In addition, sustainable land-use planning that limits repeated soil disturbance, particularly in areas with high *K* values, is essential to prevent ongoing degradation.

Although RUSLE–GIS provides a useful first-order approximation of spatial erosion patterns, future work should integrate more detailed approaches. Field-based sediment

measurements, sediment-delivery modelling, and physically based hydrological–erosion models would help validate and refine RUSLE outputs, thereby improving the reliability of conservation recommendations.

Comparative assessments with recent studies underscore both the strengths and limits of our approach. Wei et al. (2024), for example, modified RUSLE to incorporate seasonal snow cover in the Tianshan high-mountain environment, where snowmelt and ridge-zone processes drive exceptionally high erosion rates. The markedly lower values obtained in the UBW reflect its gentler terrain and semi-arid climate, where snow-related controls are minimal and the standard RUSLE formulation performs more consistently. In Didi et al. (2025), very high soil loss values were observed in steep, sparsely vegetated mountain terrain, whereas in our basin the maximum estimated losses ($\sim 33 \text{ t ha}^{-1} \text{ yr}^{-1}$) remain comparatively lower and more diffusely distributed across piedmonts and slope margins. Similarly, Thomas et al. (2018) reported much higher mean gross erosion rates in a tropical mountain basin and employed a sediment-delivery component not included in our model framework. Their findings highlight the influence of intensive land-use practices on sediment transport, whereas in the UBW erosion patterns are driven predominantly by intrinsic environmental factors such as rainfall variability, soil erodibility, and discontinuous vegetation cover.

5 Conclusion, recommendations and outlook perspectives

This study provides a comprehensive evaluation of soil erosion dynamics in the UBW through the integration of the RUSLE model with GIS and field-based analyses. By combining quantitative modeling with spatial data, the research quantified the influence of five key parameters: rainfall erosivity (*R*), soil erodibility (*K*), topographic factor (*LS*), vegetation cover (*C*), and conservation practices (*P*); which collectively determine the spatial variability of erosion across the UBW.

The results reveal a pronounced spatial heterogeneity in soil loss rates, reflecting the complex interplay between natural and anthropogenic factors. More than two-thirds of the watershed is characterized by low to moderate erosion potential, with estimated soil losses below 6 t/ha/year, primarily in gently sloping areas and zones with stable vegetation cover. In contrast, the northern and southwestern sectors exhibit the highest erosion intensities, exceeding 33 t/ha/year over approximately 9% of the total area. These critical zones correspond to steep topographic gradients, friable geological formations, and reduced vegetative protection, conditions that enhance the impact of intense rainfall events and accelerate surface runoff and sediment detachment.

The integrated RUSLE–GIS approach proved effective in capturing the spatial distribution and magnitude of soil erosion, offering a valuable decision-support framework for land and water management. The derived maps not only identify the most erosion-prone areas but also provide essential insights into the underlying processes driving land degradation. These findings underscore the importance of adopting targeted soil and water conservation strategies, including reforestation, contour farming, terracing, and slope stabilization, particularly in high-susceptible zones.

At last, this work highlights the urgent need for sustainable land-use planning and adaptive watershed management to mitigate soil loss and preserve ecosystem functions. Future research should aim to refine erosion modeling by integrating temporal datasets, sediment yield measurements, and hydrological simulations, thereby improving predictive accuracy and supporting long-term resilience of the UBW under changing climatic and land-use conditions.

The results of this study provide a scientific basis for prioritizing soil and water conservation interventions within the semi-arid environments of the MENA region. By identifying erosion-prone zones with spatial precision, the findings enable policymakers and local planners to implement targeted measures that optimize resource allocation and reduce land degradation risks. Integrating RUSLE–GIS assessments into regional land management programs would strengthen soil conservation planning, improve agricultural productivity, and enhance watershed resilience to climatic extremes. Furthermore, the methodological framework developed here can be replicated in other semi-arid regions facing similar geomorphological and hydrological challenges, thereby contributing to broader sustainable land management efforts.

Data availability statement

The original contributions presented in the study are included in the article/supplementary material, further inquiries can be directed to the corresponding author.

Author contributions

AG: Methodology, Data curation, Writing – original draft, Investigation, Conceptualization. RH: Writing – review and editing, Validation, Methodology, Supervision, Conceptualization. KF: Writing – original draft, Visualization, Software, Validation, Conceptualization, Supervision. SA: Conceptualization, Resources, Writing – original draft, Formal Analysis. EA: Data curation, Methodology, Writing – original draft. MA: Methodology,

Conceptualization, Resources, Writing – original draft. JA: Writing – original draft, Conceptualization, Software. CF: Writing – review and editing, Validation, Project administration, Visualization.

Funding

The author(s) declared that financial support was received for this work and/or its publication. Princess Nourah bint Abdulrahman University Researchers Supporting Project number (PNURSP 2025R911), Princess Nourah bint Abdulrahman University, Riyadh, Saudi Arabia.

Conflict of interest

The author(s) declared that this work was conducted in the absence of any commercial or financial relationships that could be construed as a potential conflict of interest.

Generative AI statement

The author(s) declared that generative AI was not used in the creation of this manuscript.

Any alternative text (alt text) provided alongside figures in this article has been generated by Frontiers with the support of artificial intelligence and reasonable efforts have been made to ensure accuracy, including review by the authors wherever possible. If you identify any issues, please contact us.

Publisher's note

All claims expressed in this article are solely those of the authors and do not necessarily represent those of their affiliated organizations, or those of the publisher, the editors and the reviewers. Any product that may be evaluated in this article, or claim that may be made by its manufacturer, is not guaranteed or endorsed by the publisher.

References

- Abdo, H. G. (2022). Evaluating the potential soil erosion rate based on RUSLE model, GIS, and RS in Khawabi river basin, Tartous, Syria. *DYSONA-Applied Sci.* 3 (1), 24–32. doi:10.30493/DAS.2021.311044
- Abgrami, A., Zhang, W., Mao, H., and Wang, L. (2025). GIS-based comparative landslide susceptibility mapping for Kelardasht county with ANN, SVM and RF models. *Civ. Geoengin. Lett.*, 2(1), 100028. doi:10.22034/CGEL.2.1.e100028
- Ahadi, E., and Rosta, D. A. (2024). Landslide susceptibility analysis for Azershahr region using SVM and logistic regression methods. *Civ. Geoengin. Lett.* 1 (2), e100022. doi:10.22034/CGEL.1.2.e100022
- Ait Haddou, M., Kabbachi, B., Aydda, A., Bouchriti, Y., and Mabrouki, J. (2024). RUSLE-based model for soil loss modeling and water erosion susceptibility mapping in the Issen basin (west-central of Morocco). *Iran. J. Earth Sci.* 16 (4), 1–14. doi:10.57647/j.ijes.2024.1604.21
- Alioune, M. A. E. M., Hadji, R., Barbieri, M., Gentilucci, M., and Hamed, Y. (2025). Integrated analysis of erosion and flood susceptibility in the Gorgol Basin, Mauritania. *Water* 18 (1), 34. doi:10.3390/w18010034
- Arnoldus, H. M. J. (1980). "An approximation of the rainfall factor in the universal soil loss equation," in *Assessment of erosion*. M. De Boodt, and D. Gabriels (Chichester, UK: John Wiley and Sons), 127–132.
- Benaïche, M., Mokhtari, E., Berghout, A., Abdelkebir, B., and Engel, B. (2024). Identification of soil erosion-susceptible areas using revised universal soil loss equation, analytical hierarchy process and the fuzzy logic approach in sub-watersheds boussellam and K'sob Algeria. *Environ. Earth Sci.* 83 (1), 34. doi:10.1007/s12665-023-11339-7
- Benmarce, K., Hadji, R., Hamed, Y., Zahri, F., Zighmi, K., Hamad, A., et al. (2023). Hydrogeological and water quality analysis of thermal springs in the Guelma region of North-Eastern Algeria: a study using hydrochemical, statistical, and isotopic approaches. *J. Afr. Earth Sci.* 205, 105011. doi:10.1016/j.jafrearsci.2023.105011
- Benmarce, K., Zighmi, K., Hadji, R., Hamed, Y., Gentilucci, M., Barbieri, M., et al. (2024). Integration of GIS and water-quality index for preliminary assessment of groundwater suitability for human consumption and irrigation in semi-arid region. *Hydrology* 11 (5), 71. doi:10.3390/hydrology11050071

- Borrelli, P., Lugato, E., Montanarella, L., and Panagos, P. (2017). A new assessment of soil loss due to wind erosion in European agricultural soils using a quantitative spatially distributed modelling approach. *Land Degrad. and Dev.* 28 (1), 335–344. doi:10.1002/ldr.2588
- Bueno-Hurtado, P., and Seidou, O. (2024). Empirical and physical modelling of soil erosion in agricultural hillslopes. *J. Hydrology Hydromechanics* 72 (3), 279–291. doi:10.2478/johh-2024-0017
- Cemiloglu, A., Zhu, L., Mohammednour, A. B., Azarafza, M., and Nanehkar, Y. A. (2023). Landslide susceptibility assessment for Maragheh County, Iran, using the logistic regression algorithm. *Land*, 12(7), 1397. doi:10.3390/land12071397
- Chakraborty, R., Ali, T., Pal, T., Pande, C. B., Elaksher, A. F., and Abioui, M. (2025). Climate change and land use dynamics: modeling soil erosion scenarios to achieve sustainable development goals. *Earth Syst. Environ.*, 1–26. doi:10.1007/s41748-025-00631-0
- Chang-guang, W. U., Sheng, L., Hua-dong, R. E. N., Xiao-hua, Y. A. O., and Zi-jie, H. U. A. N. G. (2012). Quantitative estimation of vegetation cover and management factor in USLE and RUSLE models by using remote sensing data: a review. *Yingyong Shengtai Xuebao* 23 (6), 1728–1732.
- Charef, K., Saafadi, L., Mouhir, L., Ouallali, A., Laabou, K., and Rherari, A. E. (2025). Soil water erosion in Morocco: a systematic review of modelling and prediction techniques. *Environ. Monit. Assess.* 197 (8), 950. doi:10.1007/s10661-025-14401-y
- Dahoua, L., Yakovitch, S. V., Hadji, R., and Farid, Z. (2017). “Landslide susceptibility mapping using analytic hierarchy process method in BBA-Bouira region, case study of east-west highway, NE Algeria,” in *Euro-mediterranean conference for environmental integration* (Cham: Springer International Publishing), 1837–1840.
- Didi, S., El Bouste, S., Hilali, A., Benmoussa, A., Hili, A., Ouakhir, H., et al. (2025). Modeling soil degradation in a semi-arid region using GIS techniques and the RUSLE model: case study of the Hassan Addakhil dam watershed. *J. Sediment. Environ.* 10, 589–604. doi:10.1007/s43217-025-00241-w
- Efthimiou, N., Lykoudi, E., and Psomiadis, E. (2020). Inherent relationship of the USLE, RUSLE topographic factor algorithms and its impact on soil erosion modelling. *Hydrological Sci. J.* 65 (11), 1879–1893. doi:10.1080/02626667.2020.1784423
- Fadl, M. E., Zekari, M., Labad, R., Faqeh, K. Y., Abou El-Fadl, D. M., Zahra, W. R., et al. (2025). Integrating RUSLE, AHP, GIS, and cloud-based geospatial analysis for soil erosion assessment under mediterranean conditions. *Sci. Rep.* 15, 38494. doi:10.1038/s41598-025-22503-3
- Foster, G. R., Weesies, G. A., Renard, K. G., Porter, J. P., and Yoder, D. C. (1997). *Support practice factor (P). A guide to conservation planning with the revised soil loss equation (RUSLE)*. Agriculture Handbook, 703.
- Foster, G. R., Toy, T. E., and Renard, K. G. (2003). “Comparison of the USLE, RUSLE 1 and RUSLE 2 for application in the highly disturbed lands,” in *First interagency conference*, Benson, 27–30, 154–160.
- Gezici, K., Şengül, S., and Kesgin, E. (2025). Assessment of soil erosion risk in the mountainous region of northeastern Turkey based on the RUSLE model and CMIP6 climate projections. *Environ. Earth Sci.* 84, 167. doi:10.1007/s12665-025-12184-6
- Ghosal, K., and Das Bhattacharya, S. (2020). A review of RUSLE model. *J. Indian Soc. Remote Sens.* 48 (4), 689–707. doi:10.1007/s12524-019-01097-0
- Guche, M. S., Geremew, G. B., and Ayele, E. G. (2024). GIS-Based soil erosion dynamics modeling by RUSLE at watershed level in hare watershed, rift valley basin, Ethiopia. *Appl. Environ. Soil Sci.* 2024 (1), 9916448. doi:10.1155/2024/9916448
- Hadji, R., Chouabi, A., Gadri, L., Rais, K., Hamed, Y., and Boumazbeur, A. (2016). Application of linear indexing model and GIS techniques for the slope movement susceptibility modeling in bousselam upstream basin, Northeast Algeria. *Arabian J. Geosciences* 9 (3), 192. doi:10.1007/s12517-015-2169-9
- Hadji, R., Taib, H., Hamed, Y., Yahiaoui, S., and Bedri, K. (2025). Morphometric and land use integration for erosion susceptibility assessment in the Ma labiod watershed, NE Algeria, using a compound prioritization framework. *J. Afr. Earth Sci.* 232, 105831. doi:10.1016/j.jafrearsci.2025.105831
- Hag Husein, H., Kalkha, M., Baladia, R., Al-Sarem, A., Bäuml, R., Sahwan, W., et al. (2024). Soil erosion assessment in the rainy mountainous areas of the eastern mediterranean. A case study of the El-Sarout watershed. *Environ. Dev. Sustain.* doi:10.1007/s10668-024-05744-6
- Hamad, A., Hadji, R., Boubaya, D., Brahmi, S., Baali, F., Legrioui, R., et al. (2021). Integrating gravity data for structural investigation of the Youkous-Tebessa and Foussana-Talah transboundary basins (North Africa). *Euro-Mediterranean J. Environ. Integration* 6 (2), 62. doi:10.1007/s41207-021-00270-7
- Hamed, Y., Redhaouia, B., Sâad, A., Hadji, R., Zahri, F., and Zighmi, K. (2017). Hydrothermal waters from karst aquifer: case study of the Trozza basin (Central Tunisia). *J. Tethys* 5 (1), 33–44.
- Hamed, Y., Hadji, R., Ahmadi, R., Ayadi, Y., Shuhab, K., and Pulido-Bosch, A. (2024). Hydrogeological investigation of karst aquifers using an integrated geomorphological, geochemical, GIS, and remote sensing techniques (Southern Mediterranean Basin—Tunisia). *Environ. Development Sustainability* 26 (3), 6943–6975. doi:10.1007/s10668-023-02994-8
- Hamed, A., Nejhad, S. M., and Mofrad, H. H. (2025). AHP-based susceptibility Analysis for Landslides in Fuman County, northwestern Iran. *Civ. Geoengineering Lett.* 2 (1), e100030. doi:10.22034/CGEL.2.1.e100030
- Hammad, A. A., Lundekvam, H., and Børresen, T. (2004). Adaptation of RUSLE in the eastern part of the Mediterranean region. *Environ. Manage* 34 (6), 829–841. doi:10.1007/s00267-003-0296-7
- Hateffard, F., Mohammed, S., Alsafadi, K., Enaruvbe, G. O., Heidari, A., Abdo, H. G., et al. (2021). CMIP5 climate projections and RUSLE-based soil erosion assessment in the central part of Iran. *CMIP5 Climate Projections RUSLE-based Soil Erosion Assessment Central Part Iran. Sci. Rep.* 11 (1), 7273. doi:10.1038/s41598-021-86618-z
- Huang, D., Su, L., Zhou, L., Tian, Y., and Fan, H. (2023). Assessment of gully erosion susceptibility using different DEM-derived topographic factors in the black soil region of Northeast China. *Int. Soil Water Conservation Res.* 11 (1), 97–111. doi:10.1016/j.iswcr.2022.04.001
- Kalman, R. (1967). *Le facteur climatique de l'érosion dans le bassin versant du Sebou, Maroc*. Projet Sebou, 32.
- Ketema, A., and Dwarakish, G. S. (2021). Water erosion assessment methods: a review. *ISH J. Hydraulic Eng.* 27 (4), 434–441. doi:10.1080/09715010.2019.1567398
- Khanchoul, K., Selmi, K., and Benmarce, K. (2020). Assessment of soil erosion by RUSLE model in the mellegue watershed, northeast of Algeria. *Environ. and Ecosyst. Sci.* 4 (1), 15–22. doi:10.26480/ees.01.2020.15.22
- Khemmal, H. Y., Hani, A., and Benmarce, K. (2025). Exploring groundwater recharge potential zones mapping in the northern upper boussellam region: a novel approach integrating TDS levels. *Appl. Water Sci.* 15 (5), 103. doi:10.1007/s13201-025-02413-5
- Kouli, M., Soupios, P., and Vallianatos, F. (2009). Soil erosion prediction using the revised universal soil loss equation (RUSLE) in a GIS framework, Chania, Northwestern Crete, Greece. *Environ. Geol.* 57 (3), 483–497. doi:10.1007/s00254-008-1318-9
- Li, A., Zhang, X. J., and Liu, B. (2021). Effects of DEM resolution on soil erosion prediction using Chinese soil loss equation. *Geomorphology* 384, 107706. doi:10.1016/j.geomorph.2021.107706
- Lizaga, I., Bagalwa, M., Latorre, B., Van Oost, K., Navas, A., Blake, W., et al. (2025). Tracing the trail of eroded fertile soils during a high intensity rainfall event: a fingerprinting study in war-torn tropical mountains. *J. Environ. Manag.* 373, 123573. doi:10.1016/j.jenvman.2024.123573
- Lo, A. W., and MacKinlay, A. C. (1985). The size and power of the variance ratio test in finite samples: a Monte Carlo investigation. *J. Econ.* 40 (2), 203–238. doi:10.1016/0304-4076(89)90083-3
- Mahleb, A., Hadji, R., Zahri, F., Boudjellal, R., Chibani, A., and Hamed, Y. (2022). Water-borne erosion estimation using the revised universal soil loss equation (RUSLE) model over a semiarid watershed: case study of Meskiana Catchment, Algerian-Tunisian border. *Geotechnical Geol. Eng.* 40 (8), 4217–4230. doi:10.1007/s10706-022-02152-3
- Mebarkia, A., and Boufekane, A. (2020). Human activity impact on surface water quality in semi-arid regions: a case study of Aïnzed lake (North-East Algeria). *Water Supply* 20 (5), 1726–1744. doi:10.2166/ws.2020.083
- Mi, J., Xiao, X., Guan, Q., Wang, Q., Zhang, J., Zhang, Z., et al. (2025). Exploring the spatiotemporal distribution characteristics and driving factors of water erosion in mountain area based on RUSLE-SDR. *J. Hydrology* 649, 132451. doi:10.1016/j.jhydrol.2024.132451
- Michalopoulou, M., Depountis, N., Nikolakopoulos, K., and Boumpoulis, V. (2022). The significance of digital elevation models in the calculation of LS factor and soil erosion. *Land* 11 (9), 1592. doi:10.3390/land11091592
- Moore, I. D., and Burch, G. J. (1986). Modelling erosion and deposition: topographic effects. *Trans. ASAE* 29 (6), 1624–1630. doi:10.13031/2013.30363
- Morsli, B., Mazour, M., Arabi, M., Mededjel, N., and Roose, E. (2006). Influence of land use, soils, and cultural practices on erosion, eroded carbon, and soil carbon stocks at the plot scale in the mediterranean mountains of Northern Algeria. Soil erosion and carbon dynamics. *Adv. Soil Sci.*, 103–123.
- Nanehkar, Y. A., Licai, Z., Chen, J., Azarafza, M., and Yimin, M. (2022). Application of artificial neural networks and geographic information system to provide hazard susceptibility maps for rockfall failures. *Environ. Earth Sci.*, 81 (19), 475. doi:10.1007/s12665-022-10603-6
- Ncibi, K., Hamed, Y., Hadji, R., Busico, G., Benmarce, K., Missaoui, R., et al. (2023). Hydrogeochemical characteristics and health risk assessment of potentially toxic elements in groundwater and their relationship with the ecosystem: case study in Tunisia. *Environ. Sci. Pollut. Res.*, 1–18. doi:10.1007/s11356-022-25016-y
- Ncibi, K., Mastrocicco, M., Colombani, N., Busico, G., Hadji, R., Hamed, Y., et al. (2022). Differentiating nitrate origins and fate in a semi-arid basin (Tunisia) via geostatistical analyses and groundwater modelling. *Water* 14 (24), 4124. doi:10.3390/w14244124
- Nehai, S. A., and Guettouche, M. S. (2020). Soil loss estimation using the revised universal soil loss equation and a GIS-based model: a case study of Jijel Wilaya, Algeria. *Arabian J. Geosciences* 13 (4), 152. doi:10.1007/s12517-020-5160-z

- Panagos, P., Borrelli, P., Poesen, J., Ballabio, C., Lugato, E., Meusburger, K., et al. (2015). The new assessment of soil loss by water erosion in Europe. *Environ. Sci. Policy* 54, 438–447. doi:10.1016/j.envsci.2015.08.012
- Prasad, B., Tiwari, H. L., Garia, S., Dwivedi, V., and Mishra, K. (2024). A comparative study on the modeling of soil erosion by USLE, RUSLE, and USPED. *ISH J. Hydraulic Eng.* 30 (4), 501–510. doi:10.1080/09715010.2024.2366365
- Prasannakumar, V., Vijith, H., Abinod, S., and Geetha, N. (2012). Estimation of soil erosion risk within a small mountainous sub-watershed in Kerala, India, using revised universal soil loss equation (RUSLE) and geo-information technology. *Geosci. Front.* 3 (2), 209–215. doi:10.1016/j.gsf.2011.11.003
- Probst, J. L. (1992). Géochimie et hydrologie de l'érosion continentale. Mécanismes, bilan global actuel et fluctuations au cours des 500 derniers millions d'années. *Persée-Portail Rev. Sci. SHS* 94 (1).
- Rango, A., and Arnoldus, H. M. J. (1987). "Aménagement des bassins versants," in *Cahiers techniques de la FAO*, 36.
- Rejani, R., Rao, K. V., Shirahatti, M. S., Reddy, K. S., Chary, G. R., Gopinath, K. A., et al. (2022). Spatial estimation of soil loss and planning of suitable soil and water conservation interventions for environmental sustainability in Northern Karnataka in India using geospatial techniques. *Water* 14 (22), 3623. doi:10.3390/w14223623
- Renard, K. G., and Freimund, J. R. (1994). Using monthly precipitation data to estimate the R-factor in the revised USLE. *J. Hydrol.* 157 (1–4), 287–306. doi:10.1016/0022-1694(94)90110-4
- Rhodes, C. J. (2014). Soil erosion, climate change and global food security: challenges and strategies. *Sci. Progress* 97 (2), 97–153. doi:10.3184/003685014X13994567941465
- Römkens, M. J. M., Young, R. A., Poesen, J. W. A., McCool, D. K., El-Swaify, S. A., and Bradford, J. M. (1997). "Soil erodibility factor (K. Compilers)," in *Predicting soil erosion by water: a guide to conservation planning with the revised universal soil loss equation (RUSLE)*. Editors K. G. Renard, G. R. Foster, G. A. Weesies, D. K. McCool, and D. C. Yoder (Washington, DC, USA), 65–99. *Agric. HB703*.
- Romshoo, S. A., Yousuf, A., Altaf, S., and Amin, M. (2021). Evaluation of various DEMs for quantifying soil erosion under changing land use and land cover in the Himalaya. *Front. Earth Sci.* 9, 782128. doi:10.3389/feart.2021.782128
- Roose, E. (1977). *Erosion et ruissellement en Afrique de l'Ouest. Vingt années de mesures en petites parcelles*. ORSTOM Paris, Travaux et doc, 105.78
- Roose, E. (1994). *Introduction à la gestion conservatoire de l'eau, de la biomasse et de la fertilité des sols (GCES)*. Rome: Organisation des Nations Unies pour l'alimentation et l'agriculture (FAO). *Bull. pédologique la FAO* 70, 438.
- Rouibah, K., and Belabbas, M. (2022). Modeling and monitoring surface water dynamics in the context of climate changes using remote sensing data and techniques: case of Ain Zada dam (North-East Algeria). *Arabian J. Geosciences* 15 (9), 807. doi:10.1007/s12517-022-09910-w
- Sahli, Y., Mokhtari, E., Merzouk, B., Laignel, B., Vial, C., and Madani, K. (2019). Mapping surface water erosion potential in the Soummam watershed in Northeast Algeria with RUSLE model. *J. Mt. Sci.* 16 (7), 1606–1615. doi:10.1007/s11629-018-5325-3
- Sartori, M., Ferrari, E., M'Barek, R., Philippidis, G., Boysen-Urban, K., Borrelli, P., et al. (2024). Remaining loyal to our soil: a prospective integrated assessment of soil erosion on global food security. *Ecol. Econ.* 219, 108103. doi:10.1016/j.ecolecon.2023.108103
- Shin, G. J. (1999). "The analysis of soil erosion analysis in watershed using GIS," in *Department of civil engineering, gang-won*. National University. Ph.D. Thesis.
- Stocking, M. A., and Elwell, H. A. (1973). The soil erosion problem in the communal lands of Rhodesia. *Rhod. Agric. J.* 70, 93–105.
- Stone, R. P., and Hilborn, D. (2000). Universal soil loss equation (USLE). Ontario ministry of agriculture. *Food Rural Aff.*, 4. Factsheet No. 00-001.
- Taib, H., Hadji, R., Hamed, Y., Bensalem, M. S., and Amamria, S. (2024). Exploring neotectonic activity in a semiarid basin: a case study of the Ain Zerga watershed. *J. Umm Al-Qura Univ. Appl. Sci.* 10 (1), 20–33. doi:10.1007/s43994-023-00072-3
- Taib, H., Hadji, R., and Hamed, Y. (2025). Erosion patterns, drainage dynamics, and their environmental implications: a case study of the hammamet basin using advanced geospatial and morphometric analysis. *J. Umm Al-Qura Univ. Appl. Sci.* 11 (2), 235–250. doi:10.1007/s43994-023-00096-9
- Thomas, J., Joseph, S., Thirivikramji, K. P., Abe, G., and Kannan, N. (2012). Morphometrical analysis of two tropical mountain river basins of contrasting environmental settings, the southern Western Ghats, India. *Environ. Earth Sci.* 66 (8), 2353–2366. doi:10.1007/s12665-011-1457-2
- Thomas, J., Joseph, S., and Thirivikramji, K. P. (2018). Assessment of soil erosion in a tropical mountain river basin of the southern Western Ghats, India using RUSLE and GIS. *Geosci. Front.* 9 (3), 893–906. doi:10.1016/j.gsf.2017.05.011
- Van der Knijff, J. M., Jones, R. J. A., and Montanarella, L. (1999). *Soil erosion risk assessment in Italy. EUR 19022 EN*. Luxembourg: Office for Official Publications of the European Communities, 54. Available online at: <https://publications.jrc.ec.europa.eu/repository/handle/JRC19353>.
- Wei, W., Liu, Y., Zhang, L., and Li, L. (2024). Distribution assessment of soil erosion with revised RUSLE model in Tianshan Mountains. *J. Mt. Sci.* 21, 850–866. doi:10.1007/s11629-022-7881-9
- Wischmeier, W. H. (1959). A rainfall erosion index for a universal soil-loss equation. *Soil Sci. Soc. Am. J.* 23 (3), 246–249. doi:10.2136/sssaj1959.03615995002300030027x
- Wischmeier, W. H., and Smith, D. D. (1978). *Predicting rainfall erosion losses: a guide to conservation planning. USDA agriculture handbook*, 537. Washington, D.C.: U.S. Department of Agriculture, 58.
- Wischmeier, W. H., Johnson, C. B., and Cross, B. V. (1971). A soil erodibility nomograph for farmland and construction sites. *J. Soil Water* 2, 265.
- Yeganeh, A., Nazari, R., Zhu, D., Tagizadeh, P., and Chen, Z. (2025). Landslide Inventory Database for Hazard Assessment in the Alborz Mountains, Iran. *Civ. Geoenvironment Lett.* 2 (1), e100035. doi:10.22034/CGEL.2.1.e100035
- Yin, S., Nearing, M. A., Borrelli, P., and Xue, X. (2017). Rainfall erosivity: an overview of methodologies and applications. *Vadose Zone J.* 16 (12), 1–16. doi:10.2136/vzj2017.06.0131
- Zerouali, B., Ayek, A. A. E., Bailek, N., Kuriqi, A., Wong, Y. J., Srivastava, A., et al. (2025). RUSLE model insights for soil conservation and sustainable land use in semiarid environments. *Euro-Mediterranean J. Environ. Integration* 10 (2), 853–876. doi:10.1007/s41207-024-00664-3
- Zerzour, O., Gadri, L., Hadji, R., Mebrouk, F., and Hamed, Y. (2020). Semi-variograms and kriging techniques in iron ore reserve categorization: application at Jebel Wenza deposit. *Arabian J. Geosciences* 13 (16), 820. doi:10.1007/s12517-020-05858-x